The collapse of the spindle following ablation in S. pombe is mediated by microtubules and the motor protein dynein

Parsa Zareiesfandabadi
Department of Physics, North Carolina State University

Mary Williard Elting*
Department of Physics, North Carolina State University and
Cluster for Quantitative and Computational Developmental Biology, North Carolina State University

(Dated: October 21, 2020)

A microtubule-based machine called the mitotic spindle segregates chromosomes when eukaryotic cells divide. In the fission yeast *S. pombe* , which undergoes closed mitosis, the spindle forms a single bundle of microtubules inside the nucleus. During elongation, the spindle extends via antiparallel microtubule sliding by molecular motors. These extensile forces from the spindle are thought to resist compressive forces from the nucleus. We probe the mechanism and maintenance of this force balance via laser ablation of spindles at various stages of mitosis. We find that spindle pole bodies collapse toward each other following ablation, but spindle geometry is often rescued, allowing spindles to resume elongation and segregate chromosomes. While this basic behavior has been previously observed, many questions remain about this phenomenon's dynamics, mechanics, and molecular requirements. In this work, we find that previously hypothesized viscoelastic relaxation of the nucleus cannot fully explain spindle shortening in response to laser ablation. Instead, spindle collapse requires microtubule dynamics and is powered at least partly by the minus-end directed motor protein dynein. These results suggest a role for dynein in redundantly supporting force balance and bipolarity in the *S. pombe* spindle.

I. INTRODUCTION

The mitotic spindle, a microtubule-based cellular machine, is responsible for accurate chromosome segregation in eukaryotes. During mitosis, spindle microtubules attach to the chromosomes, align them, segregate them, and physically deliver them to the two new daughter cells, ensuring each one has exactly one copy of the genetic information of the cell encoded in the chromosomes. Accurate chromosomes segregation is an essential function for life. Missegregation leads to aneuploidy, a condition of extra or missing chromosomes, which is associated with developmental defects and cancer in multicellular organisms [1, 2]. The mitotic spindle machinery is highly conserved across eukaryotes, likely due to its critical function.

S. pombe is a useful model eukaryote with a robust and well-developed toolkit for genetic perturbation. Its geometrically simple spindle structure, which comprises a single bundle of microtubules, also makes it ideal for mechanical perturbation. *S. pombe* undergoes closed mitosis, with its nuclear envelope remaining intact during chromosome segregation. The duration and length scale of mitosis is highly uniform from cell-to-cell and can be divided into three distinct phases defined by the spindle length and rate of elongation: phase one, which includes prophase and spindle formation; phase two, which includes metaphase and anaphase A, during which spindle length remains constant at $\sim 2.5\,\mu$m; and phase three, which includes anaphase B, during which the spindle extends at a constant rate, elongating the nucleus into a dumbbell shape before it ultimately divides into two daughter nuclei [3].

Mitotic spindles are built of microtubule protein filaments, which are oriented in the spindle to form a bipolar structure. During *S. pombe* mitosis, microtubule minus ends are anchored at the microtubule-organizing centers (MTOCs), while microtubule plus ends extend into both the cytoplasm and nucleoplasm. The former population form the astral microtubules, which help to orient the spindle inside the cell. The spindle microtubules, on the other hand, remain entirely in the nucleus and are nucleated from a specialized MTOC called the spindle pole body (SPB). Two SPBs are permanently connected to the nuclear envelope throughout mitosis [4]. Three classes of spindle microtubules have been identified in *S. pombe*: those that interdigitate in the mid-zone between the SPBs; those that emanate from one SPB and terminate at the other; and those that end at the kinetochore [5], analogously to the mammalian k-fiber. Together, these microtubules and their associated proteins form a bipolar structure that ensures robust and symmetric chromosome segregation.

Several studies have shown that the spindle extension in *S. pombe* is driven by sliding apart the interdigitating antiparallel microtubules at the spindle's mid-zone via motor proteins [5–7]. Previous work directly tested this model by mechanically severing spindles via laser ablation. This work demonstrated that microtubules within the spindle (rather than astral microtubules exterior to the nucleus) generate the force of spindle elongation [8, 9]. Yet, how mechanical force-balance is main-

* Correspondence: mary.elting@ncsu.edu

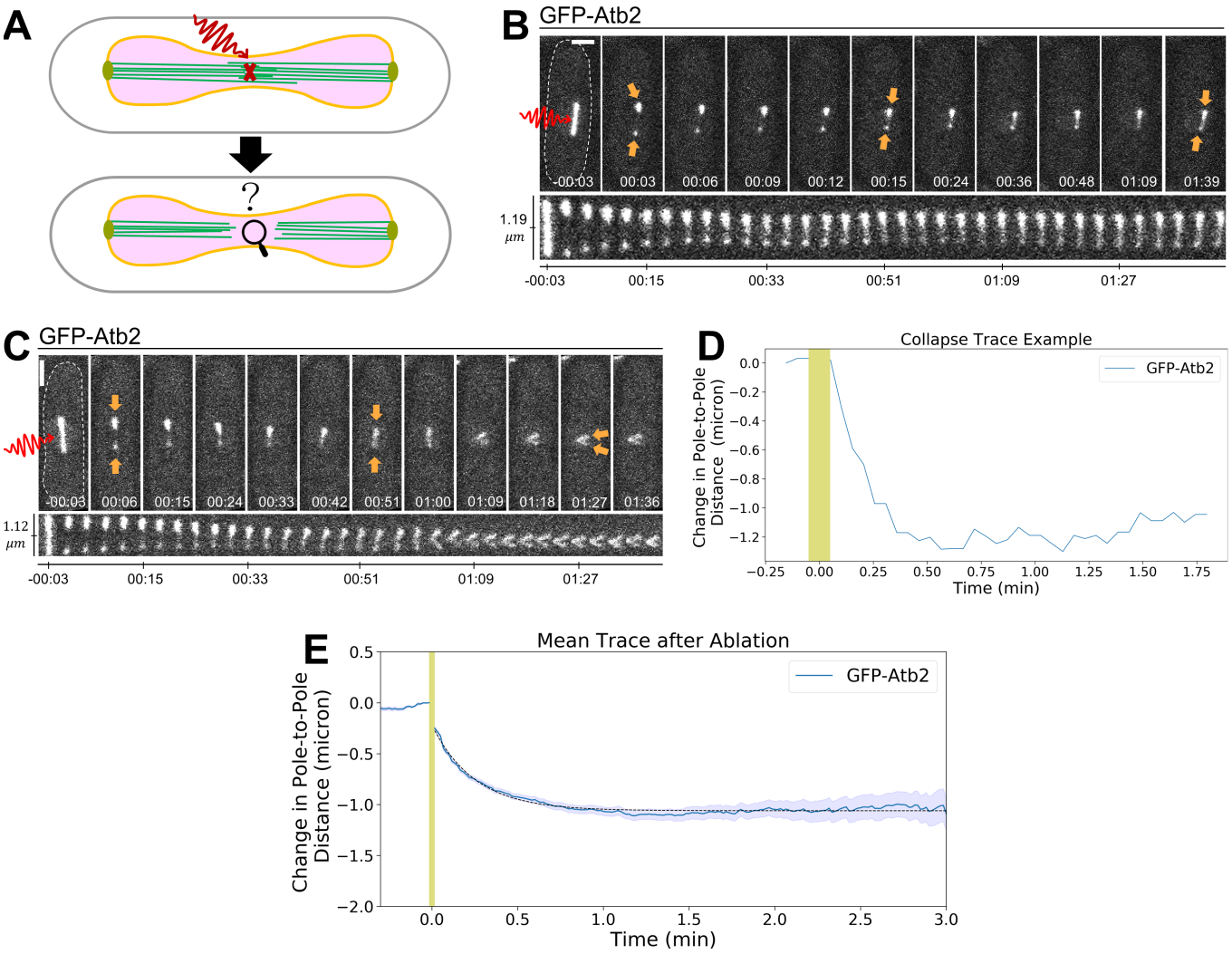

FIGURE 1. Response of the *S. pombe* mitotic spindle to laser ablation. (A) Experimental schematic. We target the spindle microtubules (green) in a *S. pombe* nucleus (magenta) for laser ablation (red X). We track the response of the spindle, the nuclear envelope (orange) and the spindle pole bodies (lime). (B) and (C) Two examples of *S. pombe* GFP-Atb2 spindles ablated near the mid-region during phase two of spindle elongation. Spindle ends (orange arrows) collapse toward each other after ablation. Top, highlighted frames; below, montage of all frames. Dashed line in first frame, cell boundary. Scale bars, $2\,\mu$m. Timestamps, min:sec. (D) Change in pole-to-pole distance over time for the example in (B). (E) The mean trace of change in pole-to-pole distance over time for $n = 185$ ablated spindles (solid blue line) and s.e.m. for all traces (blue shaded region). Black dotted line is a fit to an exponential, with amplitude $0.84 \pm 0.02\,\mu$m and time constant 0.25 ± 0.01 min. We are unable to simultaneously image during ablation, and the yellow shaded regions in (D) and (E) indicate this period.

tained amongst spindle microtubules during *S. pombe* mitosis is not yet fully clear. Importantly, these previous studies found that, following laser ablation, severed spindle fragments responded by collapsing toward each other. This work suggested that the collapse might be caused by the viscoelastic relaxation of the nuclear envelope and other materials inside the nucleus such as chromosomes, which deform in response to the extensile forces of spindle elongation [8, 9]. However, this model has not yet been tested, and nor has the molecular basis of the collapse response been found.

While viscoelastic deformation is one possible explanation for the collapse of *S. pombe* spindles in response to laser ablation, there is also a potential role for active force generation rather than passive relaxation. Indeed, force balance in the spindle generally requires the balancing of extensile forces (usually provided by plus-end directed microtubule motors that slide microtubules apart) and compressive forces (which may be provided by the chromosomes and nuclear envelope, or by minus-end directed microtubule motors).

Here, we probe the physical mechanism of the collapse of the *S. pombe* spindle in response to ablation. We show

that the viscoelastic deformation of the nucleus does not explain this phenomenon, and instead find a role for microtubule-based force generation. Finally, we find that the minus-end directed motor dynein is at least partially responsible for reconnecting the poles of ablated spindles and pulling them toward each other. While dynein is not required for mitotic spindle function in *S. pombe* [10], these results suggest a possible redundant role for dynein in ensuring mechanical force balance in the spindle.

II. RESULTS AND DISCUSSION

A. *S. pombe* spindles collapse inward following laser ablation

To probe the mechanical stability and force balance of the mitotic spindle, we ablated spindles of live *S. pombe* cells expressing GFP-Atb2 (alpha-tubulin) (Fig. 1A). Consistent with previous reports [8, 9], we found that after severing the spindle in half via laser ablation, the fragments rapidly collapse toward each other (Fig. 1B). In most cases, the two spindle fragments collapsed directly toward each other along the axis of the spindle (Fig. 1B). We also occasionally observed the fragments to rotate within the nucleus as their poles moved toward each other(Fig. 1C).

While the collapse of *S. pombe* spindles in response to laser ablation has been previously observed [8, 9], previous work did not characterize the physical or molecular mechanism underlying it. To do so, we first quantified the collapse's dynamics by tracking the end of each spindle fragment after ablation and calculating the distance between them. A typical example trace is shown in Fig. 1D, where we observe a sharp decrease in the pole-to-pole distance that begins immediately following ablation and continues for the next ~ 30 s. By averaging the trajectories for $n = 185$ ablated spindles, we determined that the average change in pole-to-pole distance over time follows an exponential relaxation response, as shown in Fig. 1E. (Note: for the spindle tracking, we used examples of the strain expressing GFP-Atb2 already described, GFP-Atb2 plus GFP-Cut11 strain, and GFP-Atb2 plus Hta1-mCherry strain; see below.) This mean trace fits well to an exponential function with magnitude $A = 0.84 \pm 0.02\,\mu$m and time constant $\tau = 0.25 \pm 0.01$ min (errors reported as standard deviations from the least-squares fit).

Previous work [8, 9] hypothesized that the spindle collapse in response to ablation might be caused by the viscoelastic relaxation of the nuclear envelope or chromosomes following disruption of extensile force from spindle elongation. Indeed, an exponential relaxation in response to ablation like the one we observe (Fig. 1E) is consistent with a passive viscoelastic response [11]. However, it is less clear that such a passive nuclear relaxation model could explain the spindles' rotation within the nucleus, which we would not expect to be accompanied by an overall change in nuclear shape (Fig. 1C). Thus, we set out to more directly test whether forces from either rearrangement of the chromosomes within the nucleus or the nuclear envelope could explain spindle collapse.

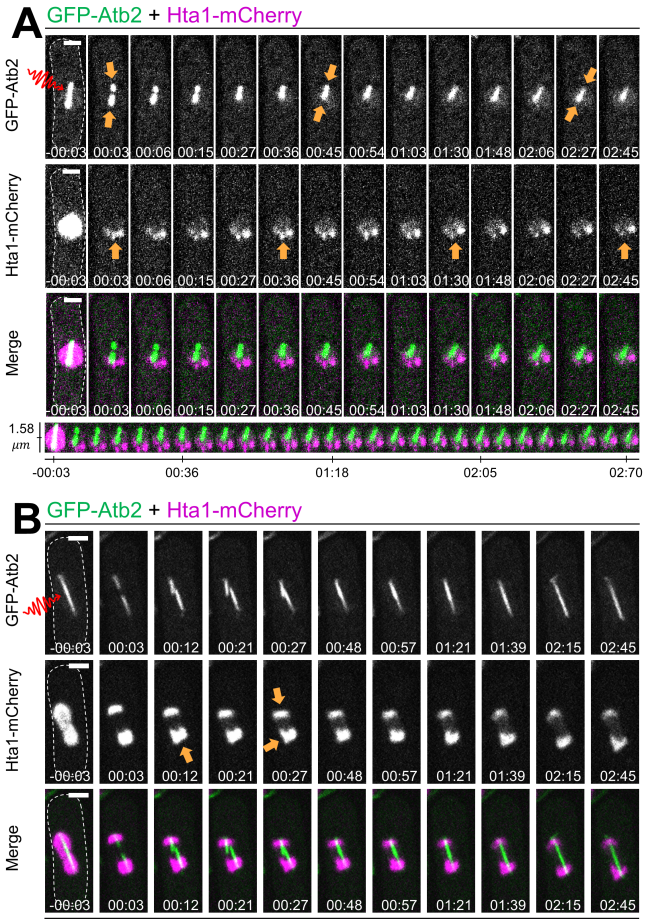

FIGURE 2. Response of histones to spindle laser ablation. (A) and (B) Two examples of *S. pombe* GFP-Atb2 plus Hta1-mCherry spindles ablated near the mid-region during early phase three and mid-phase three of spindle elongation, respectively. Arrows point to spindle ends and histones, indicating the inward collapse of the spindle and histones' movement after ablation. A montage of collapse is displayed beneath for (A). The spindle collapses inward in both examples. Scale bars, $2\,\mu$m. Timestamps, min:sec.

B. Passive viscoelastic relaxation of chromosomes does not cause the spindle's collapse

Budding yeast chromosomal DNA has been shown to act as an entropic spring [12], which therefore has the lowest energy conformation of a roughly spherical shape, and *S. pombe* chromosomes likely have similar material properties. During spindle elongation, the chromosomes are stretched out of this equilibrium state by the growing spindle. We considered whether spindle collapse might be

driven by a mechanical relaxation of the chromosomes themselves to a more spherical confirmation.

Cohesin ensures sister chromatid cohesion and resists the poleward forces that pull the sister chromatids apart [13]. When anaphase begins, cohesin is gradually degraded, allowing the sisters to separate and move to opposite spindle poles [14]. At the onset of stage three of spindle elongation, sufficient cohesin likely remains to oppose spindle elongation. This inward-directed force could cause the collapse of the spindle when it is cut. To test this hypothesis, we ablated the spindle in cells expressing GFP-Atb2 (alpha-tubulin) and hta1-mCherry (histone H2A-alpha) to observe the simultaneous response of chromosomes and the spindle to ablation (Fig. 2). If the relaxation of chromosomal DNA powers spindle collapse, we would expect to observe chromosomal rearrangements accompanying the spindle's movements.

However, following ablation, we could not detect any response of the histones in small spindles (before phase three of elongation). While bleaching of the hta1-mCherry signal by the ablation laser somewhat limits our observation immediately adjacent to the site of ablation, a detectable hta1-mCherry signal does remain following ablation (Fig. 2A and 2B). This signal did not significantly change shape in small spindles as the spindle collapsed. In other words, the spindle movements we observed seemed to occur within a largely stationary nucleus (Fig. 2A). The slight reorientation of the histones seen in Fig. 2A is not correlated with the inward movement of the collapsing spindle. While this observation is not wholly inconsistent with some movement of chromosomal DNA, if significant rearrangement occurs, it must be very localized near the site of ablation (in the area that is bleached), and thus far from the translating spindle pole bodies.

In contrast, in longer spindles that had already entered phase three of spindle elongation before ablation, we did detect an inward histone movement that accompanied the collapsing spindle (Fig. 2B). Interestingly, as the spindle collapsed, inward indentations near the ends of the spindle fragments appeared in the histone localization (see arrows in Fig. 2B). This shape suggested inward pulling on the rest of the nucleus by the spindle during collapse rather than pushing on the spindle by the chromosomes. These spindle fragments then reconnected and resumed elongation.

Overall, these data do not support a strong role for viscoelastic relaxation of the chromosomes in underlying the collapse of either short or long ablated spindles. Therefore, we next tested whether the nuclear envelope might be pushing spindle poles together after ablation.

C. Passive viscoelastic relaxation of the nuclear envelope does not cause the spindle's collapse

Particularly during phase three of spindle elongation, the *S. pombe* nucleus deforms to accommodate the lengthening spindle. This forces a change from its equilibrium spherical shape. To test whether relaxation of the nuclear envelope might have a role in spindle collapse, we repeated the ablation experiment with a strain that expresses both GFP-Atb2 to mark the spindle and nuclear envelope marker GFP-Cut11 to simultaneously observe the nuclear envelope's morphology and the spindle's collapse (Fig 3).

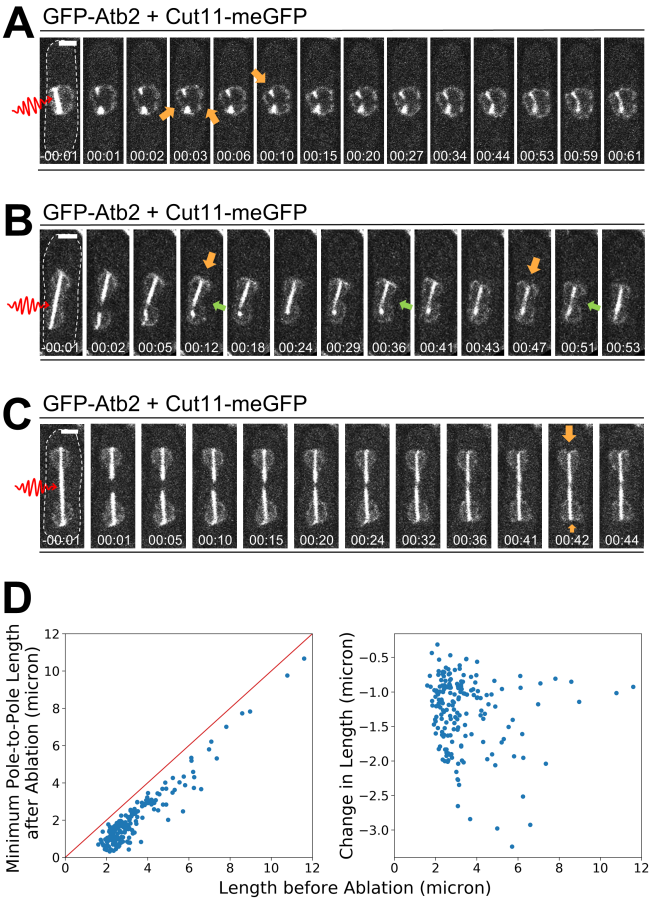

FIGURE 3. Pushing from the nuclear envelope on the spindle does not cause its collapse. (A)-(C) Three examples of *S. pombe* spindles expressing GFP-Atb2 (alpha tubulin) and Cut11-meGFP (which labels the nuclear envelope protein), ablated near the mid-region during phase two, mid-phase three, and late phase three of spindle elongation, respectively. Arrows mark the dents appearing at the nuclear envelope and cytoplasm boundary, indicating inward pulling forces after ablation. Scale bars, 2 μm. Timestamps, min:sec. The dashed line in the first frame illustrates the cell boundary for clarity. In all three examples, inward dents of nuclear envelope appear at the ends of the spindles shortly after ablation (orange arrows). In (B), green arrows highlight that the nuclear envelope keeps its dumbbell-shape after ablation. (D) Two scatter plots of $n = 185$ *S. pombe* control cells from Fig. 1 are shown. Left: scatter plot of minimum pole-to-pole length after ablation vs. length before ablation, along with a linear function showing y=x (red line). Right: scatter plot of collapsed length vs. length before ablation.

After ablation of small spindles, where the nuclear envelope is not stretched and appears spherical, the collapsing spindle appeared to exert an inward pulling force on the nuclear envelope (Fig. 2A). This presumed inward force from the collapsing spindle induces a local inward curvature of the nuclear envelope. This shape change is not consistent with pushing from the nuclear envelope, so we conclude that the nuclear envelope does not power the collapse during stage one and two of mitosis, before the nucleus has begun to elongate.

We also considered whether the nuclear envelope might play a part in the collapse when the spindle has entered phase three of elongation and begun to increase the overall dimension of the nuclear envelope. If this were the case, we would expect the indentations shown in Fig. 3A to be absent in longer spindles, and that longer spindles would have a correspondingly greater magnitude of collapse due to the larger tension forces in the nuclear envelope at this stage.

In contrast to this prediction, indentations near the poles are still present in the nuclear envelope of spindles ablated late in phase three (Fig. 3B and C). Strikingly, in addition to indentations at the ends of spindle fragments, the nuclear envelope's topology became less smooth and symmetric in some of these nuclei (Fig. 3B). Interestingly, in cells with a dumbbell-shaped nuclear envelope, the midsection's curvature remained after ablation (green arrows, Fig. 3B). This behavior suggests mechanical isolation of this region from the rest of the nuclear envelope, rather than a uniform surface tension distributed around the entire envelope.

We also examined whether the extent of spindle collapse correlated with the pre-ablation spindle length. As illustrated in Fig. 3D, we found that the minimum pole-to-pole distance correlated with the pre-cut spindle length, but that the extent of the collapse did not.

In sum, we were unable to detect a role of nuclear envelope tension in spindle collapse at any stage of mitosis.

D. Actin is not a factor in the collapse of the spindle

We next examined if actin was involved in spindle collapse by treating the cells expressing both GFP-Atb2 and Cut11-meGFP with Latrunculin A (LatA) (Fig. 4). Cells were ablated within 2-4 minutes after the addition of LatA.

As shown in Fig. 4A, we observed a very similar collapse behavior in cells treated with 100 μM LatA as in untreated spindles. When we averaged the change in pole-to-pole distance over time for $n = 28$ spindles in cells treated with 100 μM, we found that the magnitude and timescale of response were both very similar to control cells. These data suggest that actin is not a factor in spindle collapse.

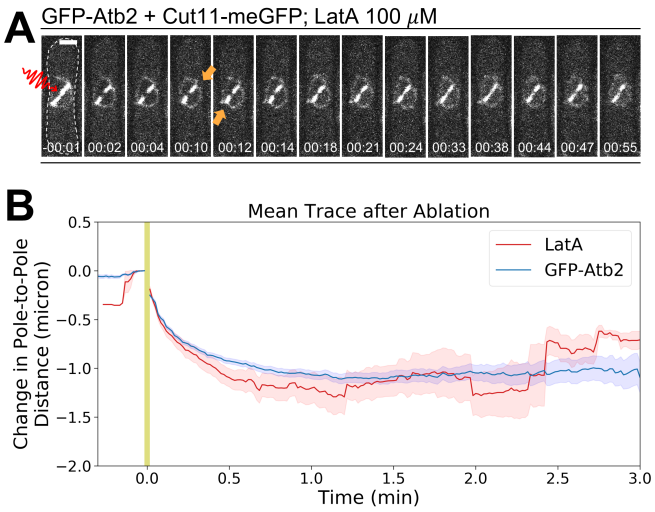

FIGURE 4. Actin depolymerization with latrunculin A does not affect spindle collapse. (A) An example of an ablated *S. pombe* spindle expressing GFP-Atb2 and Cut11-meGFP treated with 100 μM latrunculin A at during early phase three of spindle elongation. Arrows indicate nuclear envelope indentations following ablation. The dashed line indicates the cell membrane for clarity. Scale bar, 2 μm. Timestamps, min:sec. (B) The mean trace of change in pole-to-pole distance over time for $n = 28$ cells treated with 100 μM latrunculin A is plotted along with the control trace of untreated cells from Fig. 1. We are unable to simultaneously image during ablation, and the yellow shaded region indicates this period.

E. Microtubule dynamics are required for spindle collapse

After finding that passive nuclear relaxation could not explain spindle collapse, we next searched for a role of more active force generation. A rare observation shown in Fig. 5A gave a first hint at a possible role for microtubules in the process. In this example, the spindle fragments first collapsed towards each other along the spindle's main axis and then rotated. While rotating, the spindle fragments at the ablation site remained connected as each fragments' end moved closer to the other. Shortly after, the GFP signal in the region between the ends increased (orange arrow, Fig. 5A), and a new bundle of microtubules began to appear between the fragments. This observation led us to more closely investigate the role of microtubule dynamics in spindle collapse.

To test whether spindle collapse required microtubule dynamics, we treated the cells with microtubule polymerization inhibitor methyl 2-benzimidazole carbamate (MBC) before ablation (Fig. 5B and 5C). At 100 μM MBC, few cells could maintain their spindles' integrity, and all small spindles were depolymerized after the addition of MBC. However, we were still able to visualize longer spindles, which were more resistant to depolymerization. We ablated these spindles and examined their response to ablation (Fig. 5B). In this and many other

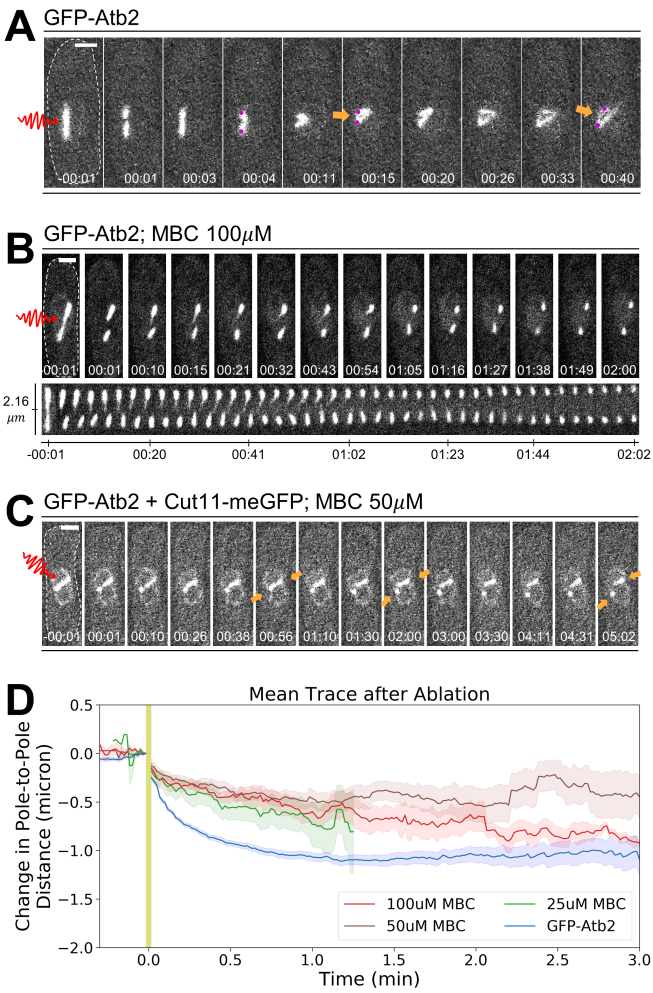

FIGURE 5. Spindle collapse after ablation requires microtubule dynamics. (A) and (B) Two examples of *S. pombe* GFP-Atb2 spindles ablated near the mid-region during phase two and mid-phase three of spindle elongation, respectively. (A) Example showing connections of off-spindle-axis microtubules during ablation. Arrows point to a bundle of microtubules. Circles (magenta) mark the supposed locations of spindle pole bodies. (B) Spindle ablation in a cell treated with 100 μM MBC, which does not lead to the spindle's collapse. A montage of the spindle following ablation is displayed beneath. (C) An example of *S. pombe* GFP-Atb2 plus Cut11-meGFP spindle ablation near one pole in a cell treated with 50 μM MBC during phase two of spindle elongation. The spindle collapses some but then seems to lose connection between the poles. Arrows illustrate the changes in the nuclear envelope following ablation. The dashed line in the first frame illustrates the cell boundary for clarity. Scale bars, 2 μm. Timestamps, min:sec. (D) The mean trace of change in pole-to-pole distance over time for $n = 7$ cells treated with 100 μM MBC, $n = 23$ cells treated with 50 μM MBC, and $n = 8$ cells treated with 25 μM MBC, is shown along with the trace of $n = 185$ untreated cells from Fig. 1 (blue line). We are unable to simultaneously image during ablation, and the yellow shaded region indicates this period.

examples, spindle collapse was notably diminished in the presence of MBC. Instead of the fragments collapsing toward each other, they appeared to be free to undergo rotational diffusion.

We also examined the response to spindle ablation at 25 μM and 50 μM MBC, where we were still able to find stage two spindles. Interestingly, we sometimes observed spindles at these concentrations that seemed to initiate collapse, with the spindle fragments reconnecting as the spindle length initially shortened, but then appeared to become detached again and diffusion apart from each other (Fig. 5C). Overall, however, collapse under this condition was lessened compared to untreated cells.

We quantified the pole-to-pole distance in ablated spindles at 25 μM, 50 μM, and 50 μM MBC (Fig. 5D). In all cases, the mean spindle length does decrease over time, but it does so much more slowly and to a smaller extent than in control spindles, indicating that spindle collapse requires microtubule dynamics. The remaining collapse in the presence of MBC may still be microtubule dependent, as we cannot completely inhibit microtubule dynamics without depolymerizing the spindle altogether.

F. Minus-end directed motor dynein contributes to the collapse of the spindle

The microtubule-dependence of spindle collapse led us to hypothesize a role for a minus-end directed microtubule motor, which might pull the spindle fragments together and shorten the pole-to-pole distance. As one of the fastest minus-end directed motor proteins in *S. pombe*[15], dynein was a natural candidate. *S. pombe* has one non-essential dynein heaving chain gene, dhc1+, which is required for the horsetail nuclear movement of meiotic prophase and meiotic recombination [10, 16]. Although evidence suggests that dynein participates during mitotic chromosomes segregation [17], a mitotic phenotype associated with the deletion of dhc1 has not been reported, and its primary functional role during mitosis remains unknown.

We examined the collapse response in *S. pombe* cells lacking the dynein heavy chain dhc1. Spindle collapse was strikingly disrupted in Dhc1Δ cells (Fig. 6). As with MBC treatment, the fragments of ablated spindles in Dhc1Δ cells often showed a prolonged diffusive search rather than a collapse (Fig. 6A and B). We also noted the lack of any further collapse at the onset of a new connection compared to wild-type spindles. On quantification, we found that the pole-to-pole distance in Dhc1Δ shows a much smaller decrease following ablation than control spindles (Fig. 6C). Thus, dynein plays an important role in powering the collapse of the *S. pombe* spindle in response to ablation. This role is likely through minus-end directed dynein motor activity that slides antiparallel microtubules to bring SPBs closer together following ablation.

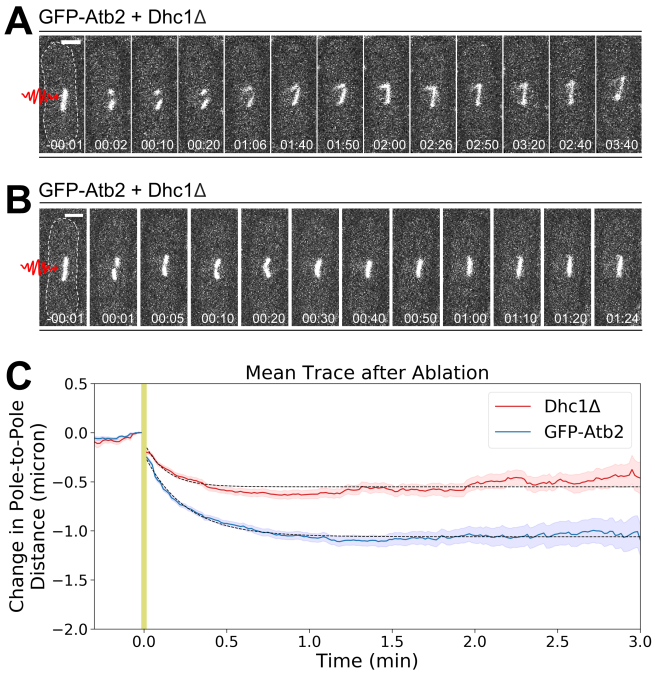

FIGURE 6. Spindles Dhc1Δ cells exhibit reduced collapse following ablation. (A) and (B) Two examples of S. pombe GFP-Atb2 plus Dhc1Δ spindles ablated near the mid-region during phase two of spindle elongation. The dashed line in the first frame illustrates the cell boundary for clarity. Scale bars, 2 μm. Timestamps, min:sec. (C) The mean trace of change in pole-to-pole distance over time for $n = 65$ ablated spindles in GFP-Atb2 plus Dhc1Δ cells is plotted (solid red line). Black dotted line is a fit to an exponential, with amplitude $0.45 \pm 0.05\,\mu$m and time constant 0.13 ± 0.02 minute. We also plot the analogous mean trace and exponential fit for $n = 185$ control untreated cells from Fig. 1 for comparison (blue). We are unable to simultaneously image during ablation, and the yellow shaded region indicates this period.

While a role for dynein in spindle collapse is clear, we do note that Dhc1Δ cells still demonstrate some degree of spindle collapse, so it must not be the only contributor. There are a few potential explanations for this result. First, it may be that there is redundancy between multiple minus-end directed microtubule motors, of which dynein is not the only example in *S. pombe* . Alternatively, we cannot fully exclude the possibility that viscoelastic relaxation of the nucleus or nuclear envelope, while not primarily responsible for it, may make some contribution to the collapse.

III. MATERIALS AND METHODS

A. Strains and cell culture

Fission yeast *Schizosaccharomyces pombe* strains used in this study were: PZ2 h+ GFP-atb2:kanMX ade6- leu1-32 ura4-D18 (from FC2861, gift of Fred Chang); PZ11 h+ hta1-mCherry:kanMX GFP-atb2:kanMX ade6- leu1-32 ura4- (from FC2859, gift of Fred Chang); PZ20 h+ nmt41-GFP-abt2-hpnMX6 + Cut11-meGFP-KanMX6 (from CL579-1, gift of Caroline Laplante); and PZ36 dhc1del::KanMX leu1-32::SV40-GFP-atb2[leu1+] ade6-leu1-32 ura4-D18 his7+ (from FC2021, gift of Fred Chang). Growth conditions and media were followed as previously described [18]. For imaging, PZ20 and PZ36 were grown in YE5S liquid media for 12-24 hours, washed three times using EMM5S, and further grown for 6-18 hours in EMM5S liquid media before imgaging. PZ2 and PZ11 were grown in YE5S media for 12 to 24 hours before imaging. All cultures were grown at 25 °C with shaking by a rotating drum. All strains were grown on YE5S agar plates before starting liquid cultures. All experiments were performed at 22 °C.

B. Microtubule and actin polymerization inhibitors

For methyl 2-benzimidazole carbamate (MBC) experiments, the cell cultures were washed twice with the same growth media at different concentration levels of MBC. Latrunculin A (LatA) was added directly to the cell culture by manual pipetting. Both LatA and MBC were diluted prior to the experiments in DMSO to 2 mM and 20 mM, respectively, and kept at 4 °C. Laser ablation experiments were conducted within 2-4 minutes of drug addition. LatA and MBC were diluted in DMSO; thus, control experiments were conducted by adding DMSO alone to the cell culture before ablation. No difference in the collapse behavior was observed.

C. Spinning disk confocal fluorescent microscopy and ablation during live-cell division

A slide for imaging was prepared using a gelatin or agar pad on a microscope glass slide. Gelatin pads were made by heating 125 mg of gelatin with 500 μL of EMM5S and heated at 80 °C for 5-10 minutes using a table-top dry heat bath. Agar pads were made by melting YE + 1% agar in a microwave. In both cases, a small amount was pipetted onto a glass slide, topped with a coverslip, and allowed to cool. 1 mL of culture at log phase (verified by measuring optical density) was centrifuged at 3500 RPM using a table-top centrifuge. The supernatant was decanted, and the pellet was resuspended in 10 μL of media. 5 μL of resuspended culture was placed on the agar or gelatin pad and covered with a coverslip. Immediately before imaging, the coverslip was sealed using VALAP (1:1:1 Vaseline:lanolin:paraffin).

Live cell spinning disc confocal imaging was performed as previously described [19, 20]. Briefly, GFP imaging was performed on a Nikon Ti-E stand on an Andor Dragonfly spinning disk confocal fluorescence microscope; spinning disk dichroic Chroma ZT405/488/561/640rpc;

488nm (50 mW) diode laser (75 ms to 120 ms exposures) with Borealis attachment (Andor); emission filter Chroma ET525/50m; and an Andor iXon3 camera. Imaging was performed with a 100x 1.45 Ph3 Nikon objective and a 1.5x magnifier (built-in to the Dragonfly system). For imaging of mCherry, we used the same settings as above except for confocal excitation with 561 nm diode laser (Andor) and emission filter Chroma ET 500/50m. Frames were collected every 1-3 s for the duration of imaging.

Targeted laser ablation was performed using an Andor Micropoint attachment to the above microscope with galvo-controlled steering to deliver 10-15 ns pulses at 20 Hz using a dye laser. Two different laser dyes were used in these experiments with emission maxima at 625 nm in cells expressing GFP-Atb2 + Htl1-mCherry (PZ11) and 551 nm for all other strains (Andor). Andor Fusion software was used to control acquisition, and Andor IQ software was used to simultaneously control the laser ablation system.

D. Analysis

ImageJ was used to crop and adjust brightness and contrast in all images. ImageJ was also used to convert the cropped .tif files to .avi for further analysis (see below). For brightness and contrast, linear adjustment was used. No interpolation or compression was used at any stage.

After the initial cropping and adjustment with ImageJ, we performed all further analyses using home-built python codes using the Jupyter notebook environment. Analysis code is available upon request. Our software loaded in the cropped image stacks as .avi files. We then used our software to record the location of the distal (presumed spindle pole body) ends of the spindles by manual tracking. We calculated the end-to-end Cartesian distance over time between these two tracked ends. We averaged the end-to-end distance traces for cells of the same treatment condition to more precisely measure the dynamics of the collapse. To average traces acquired with 1 and 3 seconds intervals, we set the value of 3 seconds interval traces to be the same for 3 seconds. The mean trace was then calculated by averaging points from each trace at that time point, and the s.e.m. of all traces was calculated for each time point and used as an estimate on the error of this mean trace. The parameters, such as amplitude and τ were found by fitting an exponential to the mean curve using the $curve_fit()$ function in python.

The control mean trace of $n = 185$ cells in Fig. 1E comprises results from PZ2, PZ11, and PZ20 strains that were not treated with MBC or LatA drug. Stepwise dropoffs in Fig. 4 and Fig. 5 mean traces are caused by individual traces having different duration.

IV. ACKNOWLEDGEMENTS

We thank Eva Johannes and Mariusz Zareba of the NC State Cellular and Molecular Imaging Facility, Kerry Bloom, and members of the Elting lab for helpful discussions, and we thank Caroline Laplante and Fred Chang for helpful advice and for providing strains. PZ acknowledges funding support by the Provost's Professional Experience Program and the Office of Undergraduate Research at North Carolina State University. MWE acknowledges support by NIH 1R35GM138083.

[1] S. Santaguida and A. Amon, Nature Reviews. Molecular Cell Biology **16**, 473 (2015).
[2] V. P. Singh and J. L. Gerton, Current Opinion in Cell Biology Differentiation and disease, **37**, 9 (2015).
[3] K. Nabeshima, T. Nakagawa, A. F. Straight, A. Murray, Y. Chikashige, Y. M. Yamashita, Y. Hiraoka, and M. Yanagida, Molecular Biology of the Cell **9**, 3211 (1998).
[4] J. R. McIntosh and E. T. O'Toole, Biology of the Cell **91**, 305 (1999).
[5] R. Ding, K. L. McDonald, and J. R. McIntosh, Journal of Cell Biology **120**, 141 (1993), publisher: The Rockefeller University Press.
[6] H. Masuda, T. Hirano, M. Yanagida, and W. Z. Cande, The Journal of Cell Biology **110**, 417 (1990).
[7] A. Mallavarapu, K. Sawin, and T. Mitchison, Current Biology **9**, 1423 (1999).
[8] A. Khodjakov, S. La Terra, and F. Chang, Current Biology **14**, 1330 (2004).
[9] I. M. Tolić-Nørrelykke, L. Sacconi, G. Thon, and F. S. Pavone, Current Biology **14**, 1181 (2004).
[10] A. Yamamoto, R. R. West, J. R. McIntosh, and Y. Hiraoka, The Journal of Cell Biology **145**, 1233 (1999).
[11] P. Roca-Cusachs, V. Conte, and X. Trepat, Nat. Cell Biol. **19**, 742 (2017).
[12] P. A. Vasquez, C. Hult, D. Adalsteinsson, J. Lawrimore, M. G. Forest, and K. Bloom, Nucleic Acids Research **44**, 5540 (2016).
[13] J. L. Gerton, Genes & Development **21**, 238 (2007).
[14] P. K. Mishra, S. Ciftci-Yilmaz, D. Reynolds, W.-C. Au, L. Boeckmann, L. E. Dittman, Z. Jowhar, T. Pachpor, E. Yeh, R. E. Baker, M. A. Hoyt, D. D'Amours, K. Bloom, and M. A. Basrai, Molecular Biology of the Cell **27**, 2286 (2016).
[15] V. Ananthanarayanan, M. Schattat, S. Vogel, A. Krull, N. Pavin, and I. Tolić-Nørrelykke, Cell **153**, 1526 (2013).
[16] I. Fujita, A. Yamashita, and M. Yamamoto, Journal of Cell Science **128**, 1555 (2015), publisher: The Company of Biologists Ltd Section: Research Article.
[17] T. Courtheoux, G. Gay, C. Reyes, S. Goldstone, Y. Gachet, and S. Tournier, Biology of the Cell **99**, 627 (2007), _eprint:

https://onlinelibrary.wiley.com/doi/pdf/10.1042/BC20070047
[18] S. L. Forsburg and N. Rhind, Yeast (Chichester, England) **23**, 173 (2006).
[19] M. W. Elting, M. Prakash, D. B. Udy, and S. Dumont, Current Biology **27**, 2112 (2017).
[20] M. A. Begley, A. L. Solon, E. M. Davis, M. G. Sherrill, R. Ohi, and M. W. Elting, bioRxiv , 2020.05.19.104661 (2020), publisher: Cold Spring Harbor Laboratory Section: New Results.